DETECTOR CHARACTERIZATION ANALYSIS OF THE INITIAL LASER
INTERFEROMETER GRAVITATIONAL-WAVE OBSERVATORY (LIGO) USING
PRINCIPAL COMPONENT ANALYSIS (PCA)

By
Daniel Hartley Duddleston

A thesis submitted to the faculty of The University of Mississippi in partial fulfillment of
the requirements of the Sally McDonnell Barksdale Honors College

Oxford
May 2014

Approved by

_____
Advisor: Dr. Marco Cavaglià

_____
Reader: Dr. Lucien Cremaldi

_____
Reader: Dr. Douglass Sullivan-Gonzalez

ACKNOWLEDGEMENTS

ABSTRACT

DANIEL HARTLEY DUDDLESTON: Detector Characterization Analysis of the initial
Laser Interferometer Gravitational-Wave Observatory (LIGO) using Principal
Component Analysis (PCA)
(Under the direction of Dr. Marco Cavaglià)

The purpose of this thesis is to investigate transient noise events in data from the

initial Laser Interferometer Gravitational-Wave Observatory (LIGO) and to test detector

characterization software developed by the LIGO Scientific Collaboration (LSC).

Detector characterization is the process of identifying and removing "noise" that corrupts

the data stream of the LIGO detectors. This is vital to improving the sensitivity of the

LIGO interferometer and increasing the probability of detecting gravitational waves of

astrophysical origin. The data analyzed in this thesis were collected in 2010 during the S6

(Enhanced LIGO) science run. Two software tools, PCAT and Omega Scans, were used

to analyze the data. PCAT (Principal Component Analysis for Transients) uses a

technique based on Principal Component Analysis to identify and classify instrumental

transient noise events ("glitches"). The Omega Scans software was used in the follow-up

study of individual glitches to investigate their spectral properties. Two 8.5-hour long and

one 16.5-hour long data stretches of S6 data were analyzed. Analysis of these data

showed that PCAT correctly classifies glitches with an efficiency of about 60%.

TABLE OF CONTENTS

LIST OF TABLES AND FIGURES

LIST OF ABBREVIATIONS

LIGO   Laser Interferometer Gravitational Wave Observatory

LSC   LIGO Scientific Collaboration

PCA   Principal Component Analysis

PCAT   Principal Component Analysis for Transients

BICEP2   Background Imaging of Cosmic Extragalactic Polarization Telescope

aLIGO   Advanced LIGO

S6   LIGO Science Run 6

INTRODUCTION

1. LIGO

LIGO (Laser Interferometer Gravitational-Wave Observatory) is a gravitational wave detector network with detectors located in Livingston, Louisiana and Hanford, Washington. The ultimate goal of LIGO is to detect and study gravitational waves of astrophysical origin from events such as binary black hole or neutron star coalescence [1], supernovae [2], isolated neutron stars [3], and of cosmological origin [4]. Gravitational waves were first predicted by Albert Einstein shortly after he developed the Theory of General Relativity in 1916 and have yet to be directly detected. However, an indirect proof of their existence was obtained when Russell Hulse and Joseph Taylor showed that the orbital period of binary neutron stars PSR 1913 +16 decreases at the rate predicted by General Relativity due to the loss of energy though gravitational waves [5]. More recently, physicists at Harvard University announced in March 2014 indirect evidence of primordial gravitational waves using their BICEP2 (Background Imaging of Cosmic Extragalactic Polarization) telescope in Antarctica [6].

Figure 1: Aerial photograph of the Laser Interferometer Gravitational-Wave Observatory (LIGO) in Livingston, Louisiana

Scientists at the California Institute of Technology and the Massachusetts Institute of Technology signed a cooperative agreement with the National Science Foundation for the construction of LIGO in 1992 [7]. The LIGO project then expanded to include many other scientists across the world to form the LIGO Scientific Collaboration (LSC). The LSC provides the scientific support for the project. The initial LIGO interferometers in Livingston and Hanford operated at their design sensitivity from November 2005 to September 2007 [8]. An enhanced version of the initial LIGO detectors operated in 2009 and 2010. In October of 2010, LIGO scientists and engineers began disassembling the initial LIGO detectors and replacing them with more sensitive instruments [9]. The installation of upgraded interferometers in Livingston and Hanford began in 2011 and is scheduled to be completed in 2014. The new Advanced LIGO (aLIGO) interferometers will increase the sensitivity of the initial LIGO detectors by implementing new and improved laser optics and better noise isolation techniques [10]. Increased sensitivity of the interferometer means a larger volume of the Universe can be explored and an increased probability of detecting gravitational-wave events [11]. The data contained in this thesis is from the 2010 Enhanced LIGO science run (S6).
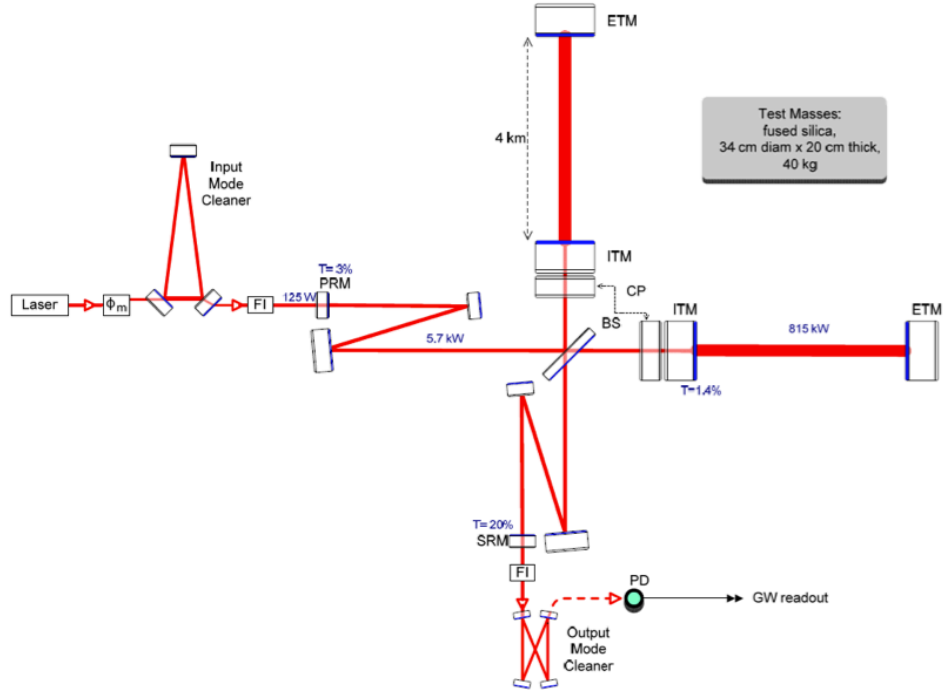
Figure 2: Schematic diagram of the Advanced LIGO interferometer showing the gravitational-wave readout channel

2. Gravitational Waves and LIGO's Design

According to Einstein's theory, mass and energy produce a curvature of four-dimensional space-time, and matter moves in response to this curvature. Gravitational waves are propagating oscillations in the space-time metric. The quadrupolar nature of gravitational waves implies that space in the plane transverse to the wave direction contracts (expands) along one direction while expanding (contracting) along the orthogonal direction [7].

Gravitational waves propagate at the speed of light but interact with matter very weakly. Rather than measuring the power, as one typically would with an electromagnetic wave, gravitational waves may be detected by measuring their "strain" $h(t)$, i.e., the change in path length ΔL over the path length L.

$$h(t) = (\Delta L)/L$$

The design of the LIGO detectors is that of a laser Michelson interferometer with added Fabry-Perot cavities [7]. This configuration allows scientists to detect gravitational waves by measuring the differential strain that the wave causes in the interferometer arms.

The strain of a typical gravitational wave of astrophysical origin is estimated to be $h \approx 10^{-21}$ or weaker. For the LIGO interferometers (arm length = 3995 m), this strain would correspond to a path length change of about or less than $1/1000^{th}$ of the diameter of a proton. Therefore, in order to detect this very small change in path length, very precise, free from outside noise, and incredibly sensitive measurements must be performed.

Since the waves are very weak, gravitational wave signals must be extracted from the instrumental and environmental "noise," such as seismic, weather, or anthropogenic activity. The LIGO interferometers are set to operate at a dark fringe (deconstructive interference of the laser). Photo-diodes at the output of the interferometer observe a gravitational wave signal as a fluctuation in the intensity of the light. The calibrated gravitational wave strain amplitude, *h(t)*, is reconstructed taking into account the frequency-dependent transfer functions of the instrument which are applied to the uncalibrated dark fringe signal [7]. Detector characterization, the process of identifying and removing the "noise" produced by varying sources of vibration, plays a crucial role in any attempt to detect gravitational wave signals.
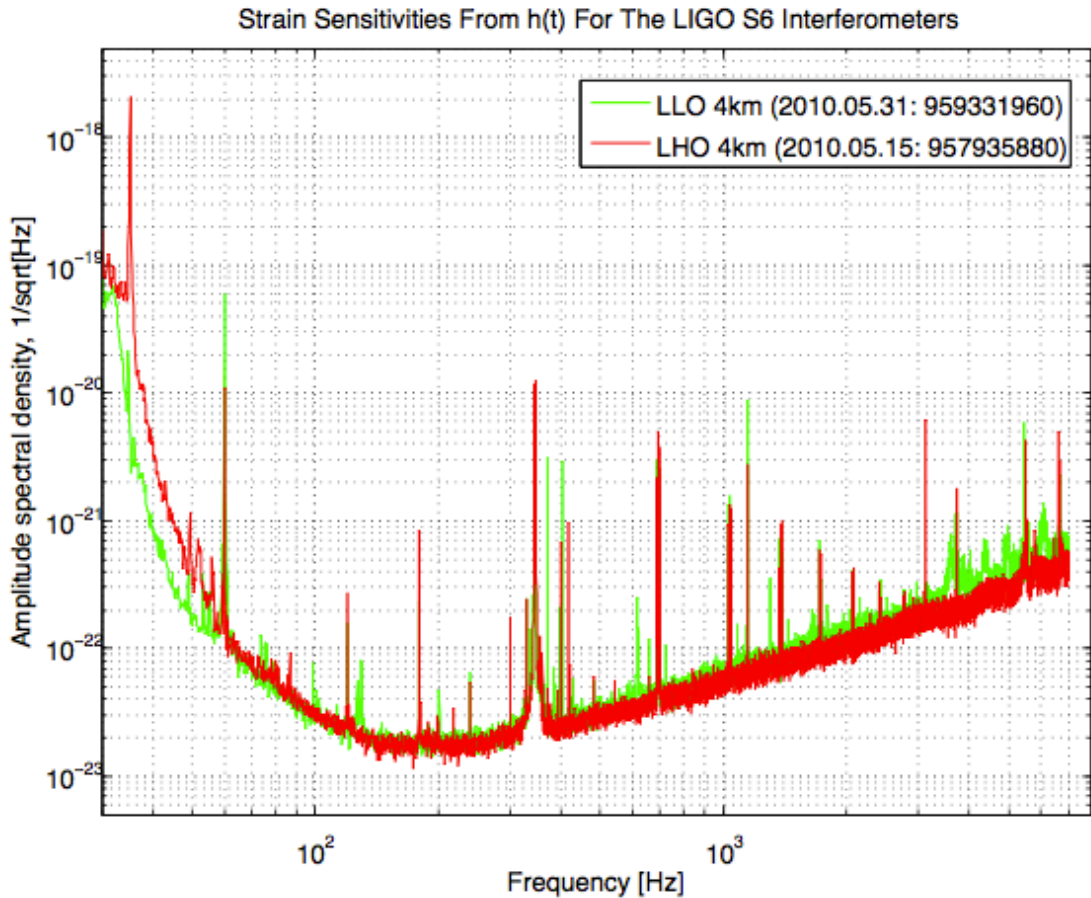
Figure 3: Typical strain sensitivities of the initial LIGO interferometers in the S6 science run [12]

To achieve the required sensitivity for detecting gravitational waves, it is necessary to identify and remove environmental disturbances, which cause unwanted strain on the laser. Therefore, the LIGO interferometers are equipped with thousands of data sensors to monitor instrumental and environmental activities. The LIGO "auxiliary channels" include microphones, seismometers, magnetometers, photo-diodes, current, and voltage monitors, etc.

Software capable of finding and classifying instrumental glitches may help to identify and remove unwanted noise in the data stream. Principal Component Analysis for Transients (PCAT) is a suite of python tools based on Principal Component Analysis

(PCA) that has been developed by the University of Mississippi LIGO group to find, characterize, and classify noise transients ("glitches") in the time and/or frequency domain(s) [13].

3. Principal Component Analysis

PCA is a technique based on an orthogonal linear transformation that transforms a set of observations of (possibly correlated) variables into another set of linearly uncorrelated variables, called Principal Components [13]. The PCAT software uses the PCA algorithm to convert a matrix of glitch observations into a set of principal component scores that can be used to identify and classify noise transients in the gravitational-wave channel and in auxiliary channels. Suppose one has n observations of m variables (in our case the observations are time series, with the variables being points in the time series). These are arranged in a data matrix $D\cdot$, where each row is an observation and each column a variable (time stamp). After the columns have been standardized, i.e., each column's mean is set to zero; one calculates the covariance matrix of D (the matrix of the covariances between each variable).

The covariance matrix is a $p \times p$ symmetric matrix, which can be diagonalized by finding a set of orthonormal eigenvectors. The basis of eigenvectors, ordered by decreasing absolute value of the corresponding eigenvalue, is called basis of "Principal Components". By projecting the original data onto the new (diagonal) basis, we obtain a new matrix, called the "Principal Component Scores matrix." The noise transients can be characterized and classified by the value of their scores [13].

Let us consider n observations of p variables, x_{ij}, $i = 1 \ldots n$, $j = 1 \ldots p$. The data matrix is defined as

$$D(\mathbf{X}_j) = \overbrace{\begin{pmatrix} x_{11} & x_{12} & \ldots & x_{1p} \\ x_{21} & \ddots & & \vdots \\ \vdots & & \ddots & \vdots \\ x_{n1} & \ldots & \ldots & x_{np} \end{pmatrix}}^{\mathbf{X}_1 \quad \mathbf{X}_2 \quad \ldots \quad \mathbf{X}_p}. \tag{1}$$

Each row (column) of the data matrix represents a different observation i (variable $\mathbf{X}_j$). The standardized data matrix $\mathbf{D}_s = D(\mathbf{X}_j^{(s)})$ is obtained by subtracting from each $\mathbf{X}_j$ its mean

$$\mathbf{X}_j^{(s)} = \mathbf{X}_j - \frac{1}{p}\sum_{i=1}^{p} x_{ij} \tag{2}$$

and replacing $\mathbf{X}_j$ with $\mathbf{X}_j^{(s)}$ in $\mathbf{D}$. The covariance matrix is defined as

$$\mathbf{\Sigma}_{jk} = \mathrm{Cov}(\mathbf{X}_j^{(s)}, \mathbf{X}_k^{(s)}), \quad j, k = 1, \ldots p. \tag{3}$$

Since the covariance matrix $\mathbf{\Sigma}$ is a $p \times p$ symmetric matrix, it can be diagonalized by the orthogonal matrix

$$\mathbf{M} = (\mathbf{u}_1 \; \mathbf{u}_2 \; \ldots \; \mathbf{u}_j \; \ldots \; \mathbf{u}_p), \tag{4}$$

where $\mathbf{u}_j$ are the orthonormal *Principal Components* eigenvectors ordered by decreasing eigenvalue absolute value. The standardized data can be projected on the new basis

$$\mathbf{S} = \mathbf{D}_s \, \mathbf{M}. \tag{5}$$

The $n \times p$ matrix $\mathbf{S}$ is called the *Score Matrix*. The coefficients of the expansion of the standardized data set w.r.t. the new basis are called *Principal Component Scores*. The original data can be retrieved from Eq. (5) by constructing the linear combination of the principal components $\mathbf{u}_j$ weighted by the corresponding principal component scores, and then inverting Eq. (2).

Figure 4: Mathematical representation of Principal Component Analysis

After data are analyzed with PCAT, another software, called Omega Scan [14], is used to provide more information on each individual glitch. "Omega Scans" are used to calculate spectrograms of the glitches, thus providing information on the amplitude and the spectral properties of the transients. While PCAT is a useful resource for finding glitches and their correlations, it is not 100% efficient. Omega Scans allow researchers to confirm the accuracy of the results that are obtained with PCAT, thus reducing the false positives of the PCA algorithm.

4. Dart Glitch Challenge

Data Quality experts in the LSC Data Characterization group found a number of problematic glitches of unknown origin in a collection of data from Enhanced LIGO,

which warranted further investigation. In particular, they identified a set of "dart" glitches as a distinct set of short-lived transients with typical frequency in the 30 to 60 Hz range, sometimes with higher frequencies up to 200 Hz. These glitches were identified due to their coupling into the main channel, L1:LSC-DARM_ERR, from which the gravitational-wave strain is obtained after calibration. Because of their characteristics, "dart" glitches provide a suitable testing bed for glitch identification and classification algorithms. Thus, a "Glitch Classification Challenge" was created to test glitch classifier methods and provide further insight on the nature of these glitches. The challenge was to test classifier methods by running the software over the S6 data, identifying "dart" glitches and separating them from the other classes of transients. This thesis reports the outcome of PCAT's attempt to resolve the challenge; two 8.5 hour-long data intervals and one 16.5 hour-long interval where "dart" glitches were known to be present were analyzed with PCAT to test the efficiency of the software in identifying and classifying the transients. Only "locked times" were analyzed by PCAT, ensuring that the instrument was "locked" and operating as it normally would to attempt to detect gravitational waves.

Date (2010)	Time (24 hr. Central Standard Time)
February 27-28	18:00-02:30 (6:00pm-2:30am)
March 11-12	18:00-02:30 (6:00pm-2:30am)
March 12-13	10:00-02:30 (10:00am-2:30am)

Table 1: Time intervals ("locked times") of data that PCAT analyzed
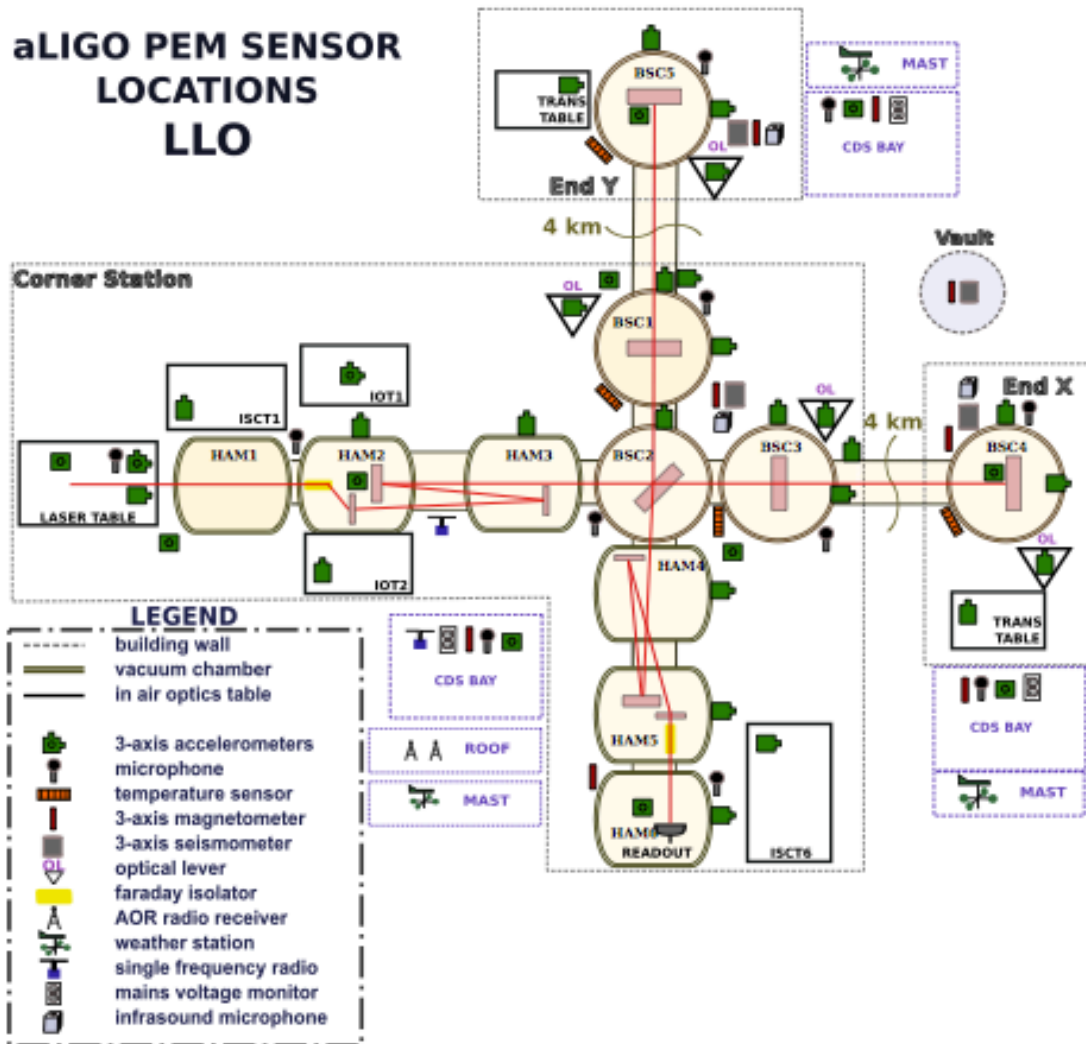
Figure 5: Schematic diagram of the aLIGO Livingston interferometer showing the auxiliary channels, which monitor environmental and instrumental noise [15]

METHODS

The main goal of "Detector Characterization" is to identify and reduce noise of non-astrophysical origin in the detector output to improve the detector's performance and sensitivity [16]. LSC researchers have developed many different and complementary software tools to help with this task [17, 18, 19, 20]. The noise hunting process that is used by these tools generally follows these steps:

1. Identify noise events in the detector's outputs (gravitational-wave or auxiliary channels)

2. Time correlate the noise with unusual detector behavior or environmental disturbances.

3. If the noise source is identified, eliminate the source of noise or excise the corrupted data from the data stream that is analyzed in searches for gravitational-wave signals.

Two of the software tools that were used in this work to characterize the detector are PCAT [13] and Omega Scans [14]. The output of PCAT includes the event times of each glitch which are identified in a given channel, their classification into distinct types based on their Principle Component Scores, and the time series, or waveforms, of each individual glitch and type representatives. Omega Scans are then used to provide complementary information on the frequency, duration, and amplitude of each individual glitch.

RESULTS

From the Enhanced LIGO S6 data spanning the intervals listed in Table 1, PCAT
identified 256 "triggers" (GPS times indicating a glitch) corresponding to disturbances
with different characteristics and of different instrumental or environmental origin. We
classified these glitches based on their spectrogram features obtained with Omega Scans
and their time series. Examples of the main classes of glitches are shown in Figures 6-11.
Of these 256 triggers, 9 were false positives. These 9 triggers were GPS times that PCAT
identified as glitches, though the Omega Scan for each trigger does not show a true
glitch. Of the remaining 247 triggers, 61 of them were multiple trigger identifications of
single glitches due to the high time resolution of the PCAT run (12 ms). However,
because PCAT identified and classified these multiple identifications into the same type
and into different types, each trigger is counted as a distinct glitch as classified by PCAT.
Therefore, due to multiple identifications of the same glitch, the number of glitches
present in the temporal distribution plots in Figures 13, 14, and 15 is $247 - 61 = 186$.

For the purposes of finding PCAT's classifying efficiency (Table 3), each
multiple identification is considered a distinct glitch. For example, if PCAT identifies 6
triggers for a single glitch, each of the 6 triggers is considered a distinct glitch classified
by PCAT. An alternative approach would be to cluster the triggers over a time window
with duration of a typical true glitch, as seen in Omega scans.

PCAT provided a breakdown of types of triggers, numbered 1 through 6, giving
the number of triggers in a type and the percentage of the total triggers a type contains.
We classified these glitches based on their spectral properties evident in Omega Scans.
Figures 6-11 give examples of the Omega spectrograms for these classes.
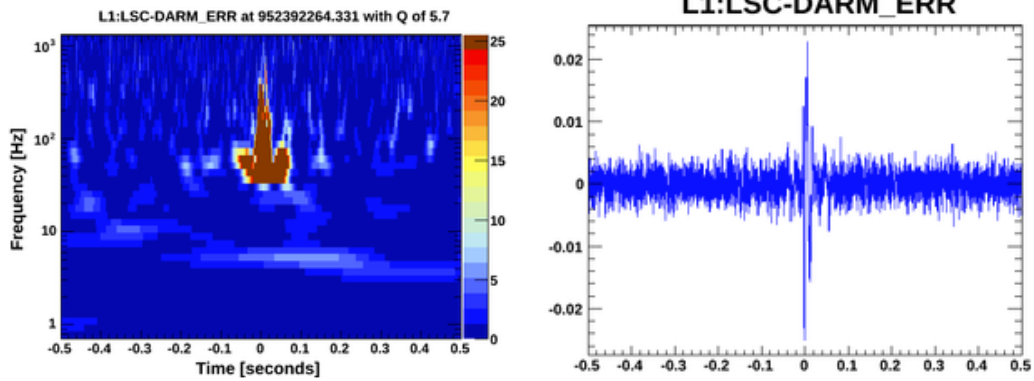
Figure 6: Example of Dart Glitch (DG). A typical dart glitch spans about 0.2 seconds in the spectrogram (left) and occupies a frequency range of 30 to 200 Hz. The characteristic shape of an DG in the whitened time series (right) is that of several high-amplitude oscillations. This category includes every DG that demonstrates the characteristics above, but does not include high amplitude dart glitches (HDGs), which show a longer duration in the spectrogram.
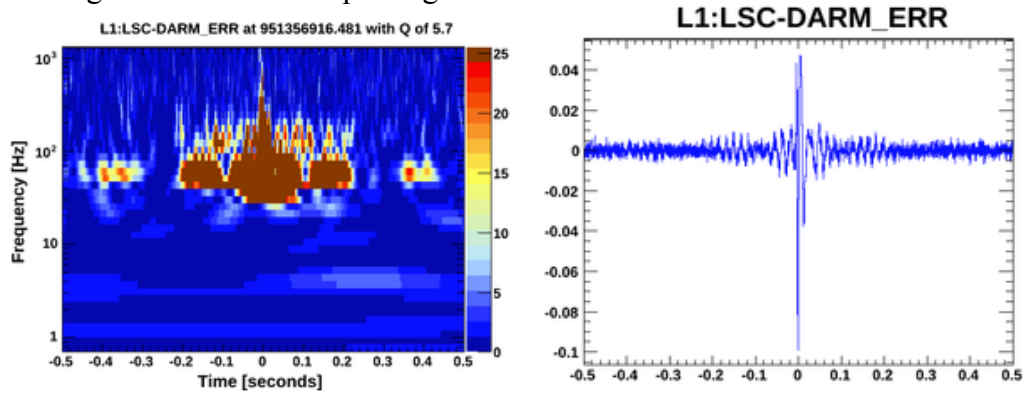
Figure 7: Example of High amplitude Dart Glitch (HDG). This glitch is essentially a louder dart glitch. It is generally categorized by PCAT in the same class as DGs. It has the characteristic DG shape, but shows a higher-amplitude in the whitened time series (right) and more noise before and after the main structure in the spectrogram (left). HDGs are characterized by the same frequency range (30-200 Hz) of lower-amplitude dart glitches.
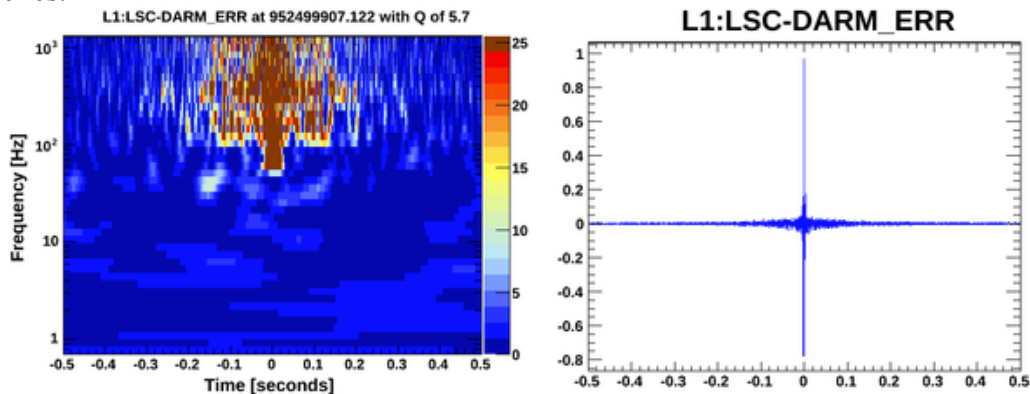
Figure 8: Example of Spike with Noise (SN). Every spike glitch shows a characteristic short-lived spike at centered higher frequencies above ~100 Hz. The louder the spike, the more noise precedes and follows the peak of the spike (right) and some are accompanied

by noise around the spike in the spectrogram (right). The time series of spike glitches display few oscillating spikes, unlike dart glitches.
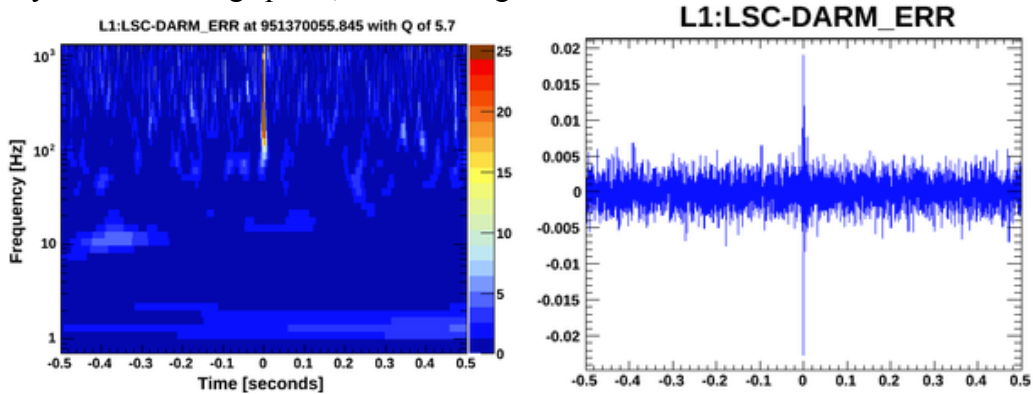
Figure 9: Example of Short Spike (SS). This is a low-noise, low amplitude (right) spike. The frequency range is the same as loud spikes (left).
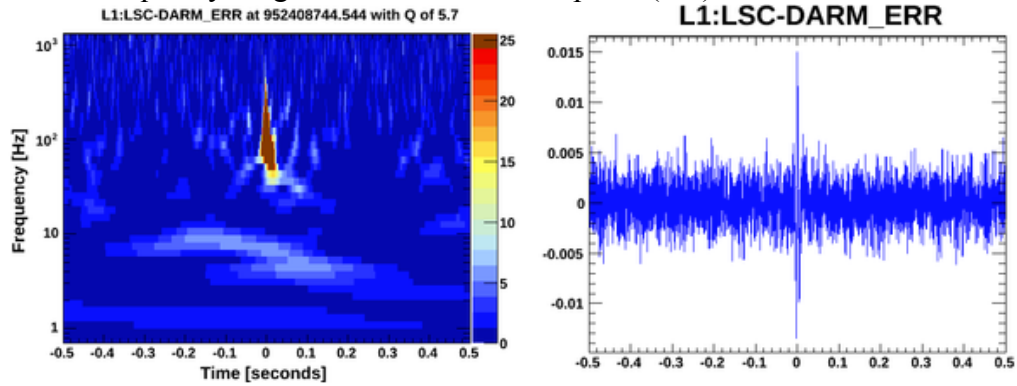
Figure 10: Example of Short Spike with Dart Glitch character (DG/SS). Several weak glitches were found in Type 6 to have features common to short spikes and low amplitude dart glitches. These glitches display more noise (left) and have a lower frequency range (60-200 Hz) than short spikes (~100+ Hz).
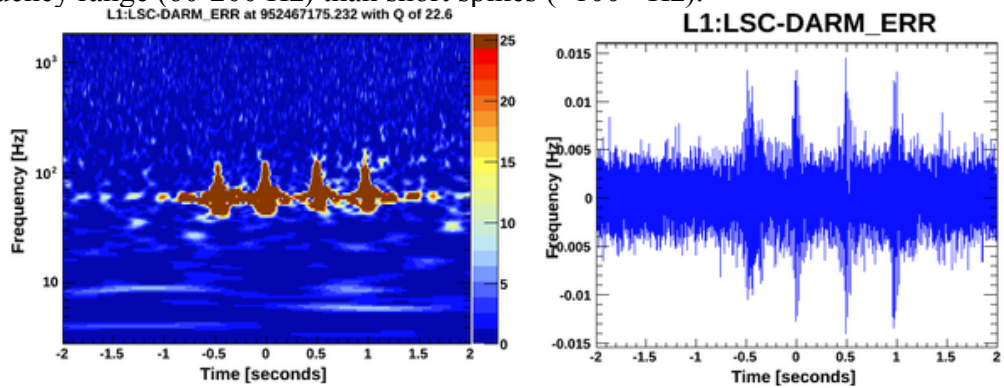
Figure 11: Example of Cross Glitches (C). This is a quadruplet cross glitch found among the data. Several cross glitches were found in the form of singlets, doublets, triplets, and quadruplets, with the singlets and doublets being more common. The typical frequency of cross glitches is in the 20-100 Hz range, and their typical duration is ~0.5 seconds (left). They are called "cross" glitches because they resemble crosses in the spectrogram (left).

Within each PCAT-identified type, there are typically glitches belonging to different classes, as identified through Omega Scans. Table 2 below shows the breakdown of glitch classes within each PCAT type. N is the number of triggers for each type PCAT identified. The abbreviations used in Table 2 are described in Figures 6-11. "OG" stands for "outlier glitch," i.e., a glitch that clearly does not belong to any other class. "FP" stands for "false positive," or a trigger identified by PCAT where no glitch is present in the Omega Scan.

Type	N	DG	HDG	DG/SS	SS	SN	C (x1)	C (x2)	C (x3)	C (x4)	OG	FP
1	9	2				1					4	2
2	9						3	3	1		2	
3	115		1		35	27		3	1		41	7
4	30	9	6				3	1	1	3	7	
5	5						2	2		1		
6	88	33	11	23	7	1					13	

Table 2: Breakdown of main glitch classes per PCAT-identified type

PCAT's efficiency (*Eff*) in classifying the transients can be defined as the number of triggers in each type "correctly classified" by the algorithm divided by the total number of triggers in that type. We define "correctly classified" triggers through the following procedure: a glitch type is matched to a glitch class when the majority of glitches in that type belong to a given class.

Eff (type) = (# of correctly classified glitches in type) / (total # of glitches in type)

PCAT classified most of the dart glitches into Types 4 and 6, cross glitches into Types 2, 4, and 5, and spike glitches into Type 3. Therefore, type 1 can be considered the outlier glitch class, type 2 the cross class I, type 3 the spike class, type 4 the dart class I, type 5 the cross class II, and type 6 the dart class II. Table 3 below shows PCAT's classifying efficiency by type.

Type (main glitch class)	Number of triggers "correctly classified" by PCAT per type	Number of triggers identified by PCAT per type	Efficiency per type *Eff (type)*
1 (Outlier)	4	9	44.4%
2 (Cross I)	7	9	77.8%
3 (Spike)	62	115	53.9%
4 (Dart I)	15	30	50.0%
5 (Cross II)	5	5	100.0%
6 (Dart II)	67	88	76.1%
Total	**160**	**256**	**62.5%**

Table 3: Efficiency of PCAT per type

The efficiency of PCAT is lowered when a large amount of outlier glitches are present. This was the case for types 3 and 6, as the algorithm of PCAT was tasked with classifying glitches with spectral properties unlike other glitches in the data. For example, PCAT identified 10 triggers for the same outlier glitch in type 3 that spanned 6 seconds in the spectrogram. Each trigger was counted as an outlier glitch, even though only one true glitch was present in the Omega Scan. For the purposes of calculating PCAT's efficiency, we must count each trigger as a distinct glitch. From investigation of the Omega Scans for those triggers though, we can then see that it is only 1 glitch. Clustering PCAT triggers as described above would increase PCAT efficiency.

Figure 12 on the following page shows the distribution of glitches in the Principal Component Score space (first two scores). The dart glitches (most of types 4 and 6) are clustered well in the blue (bottom right) and purple (2 major clusters around (-2, -2) and (2, 2)). Type 3 is the largest class of classified glitches and is strongly correlated near the origin.
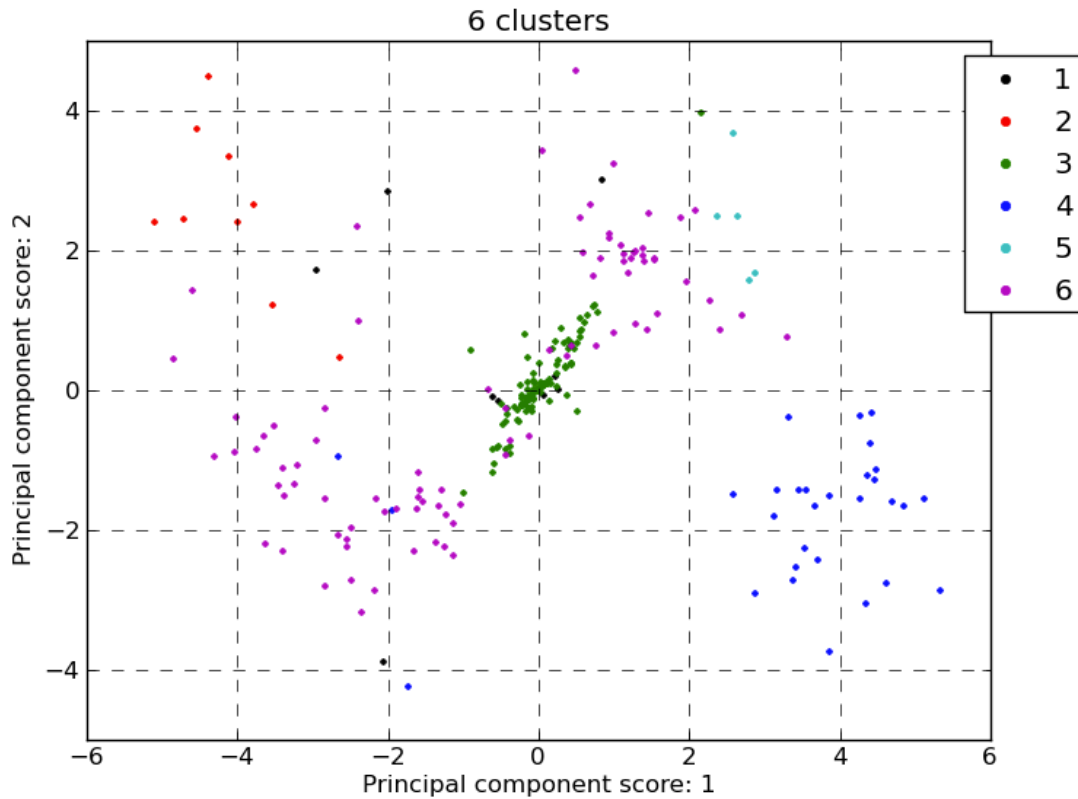
Figure 12: Triggers plotted according to their Principal Component Scores provided by PCAT

Following the classification of glitches, we investigated their temporal distribution to determine if any patterns exist. Figures 13-15 show the temporal distribution of the different glitch classes. Again, PCAT identified 256 triggers in this set of data, though only 186 true glitches were identified through Omega Scans due to multiple identifications for a single glitch and false positives.

In order to investigate the glitches on corresponding time scales, dart-like glitches are mapped in Figure 13 for the nights of February 27-28, March 11-12, and March 12-13 spanning the hours of 6:00 pm – 2:30 am CST. Figure 14 uses the same dates and times, but plots all non-dart glitches. Figure 15 shows the time interval of 10:00 – 6:00 pm on March 12 with dart-like glitches on the upper timeline and non-darts below.

16
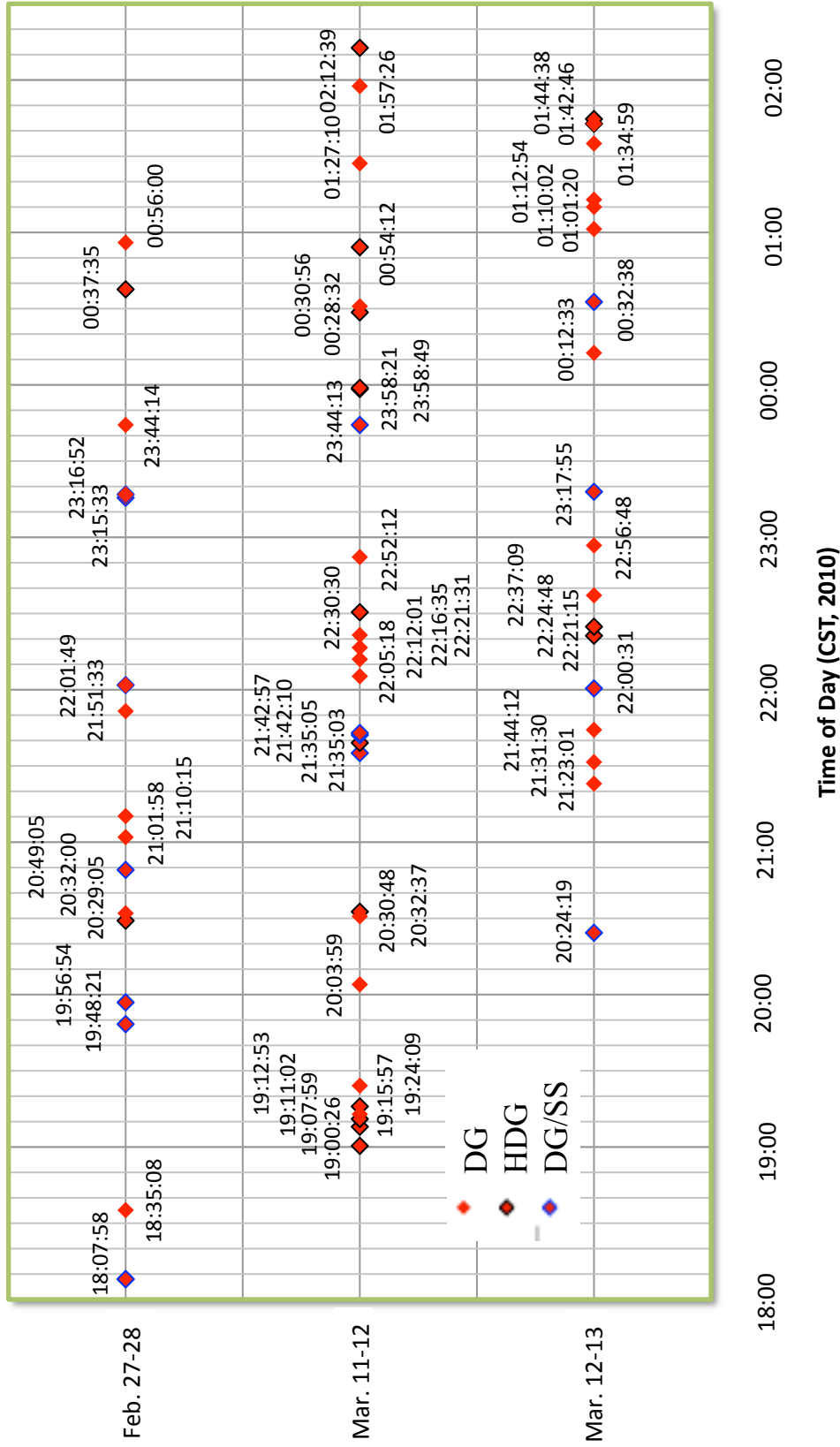
Figure 13: Temporal distribution of Dart-like Glitches (DGs, HDGs, DG/SSs) for the nights of February 27-28, March 11-12, and March 12-13

17
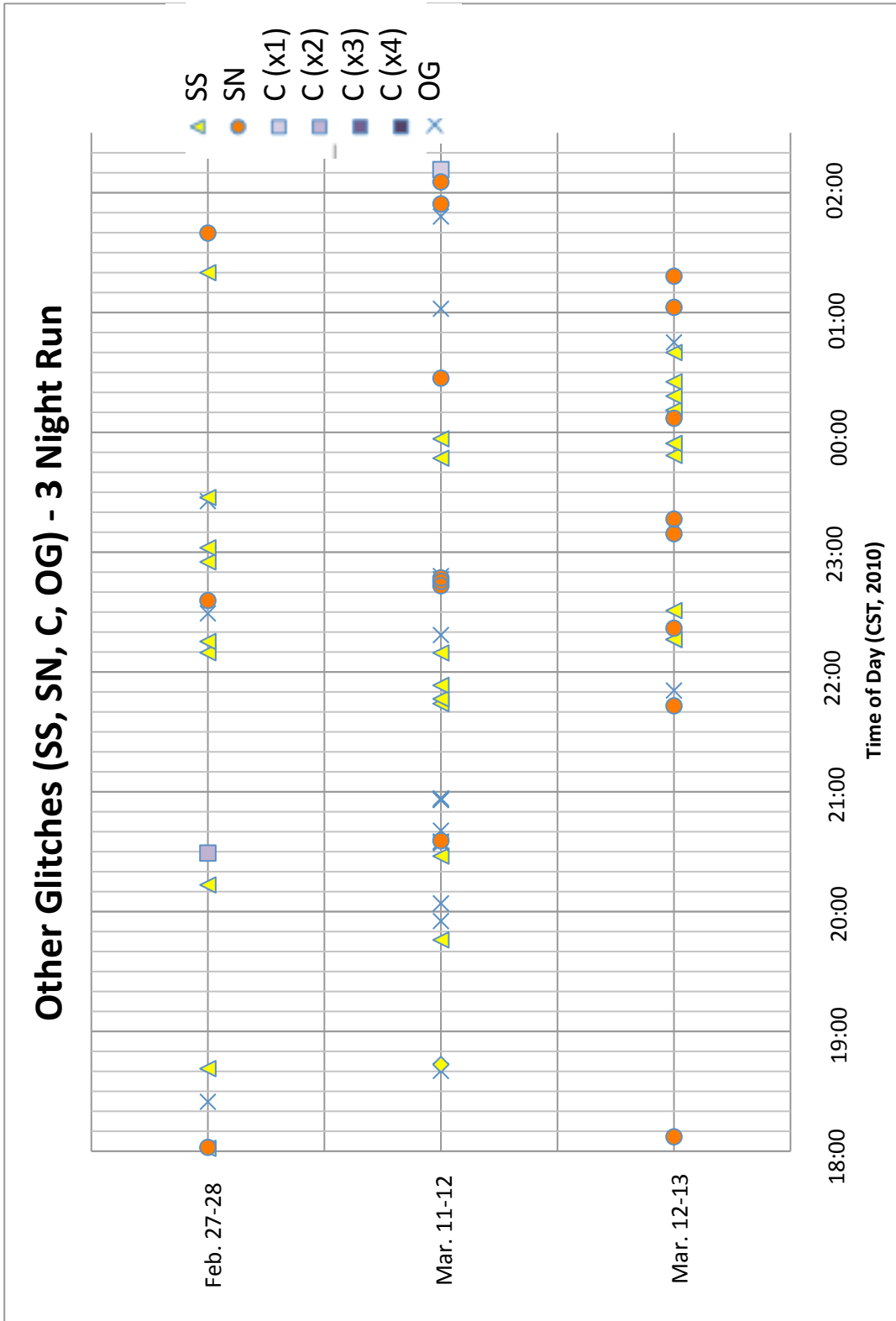
Figure 14: Temporal distribution of non-Dart Glitches (SSs, SNs, Cs, OGs) for the nights of Feb. 27-28, Mar. 11-12, and Mar. 12-13
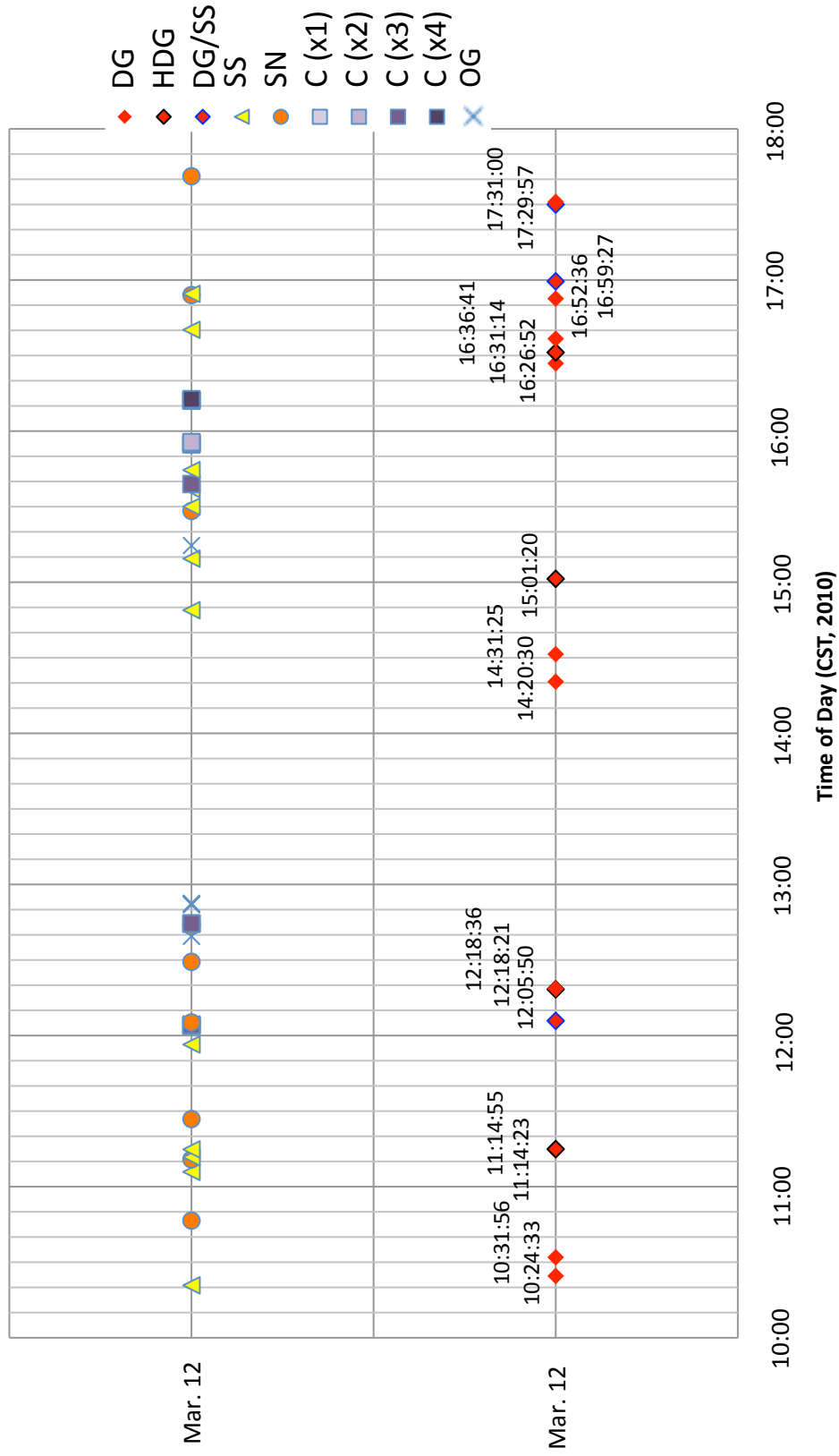
Figure 15: Temporal distribution of all glitches (Dart-like above and non-Dart below) for the hours of 10:00 am – 6:00 pm CST on March 12

19

The number and classes of glitches found for each 8.5-hour interval spanning 6:00 pm – 2:30 am CST are summarized in Table 4. The same breakdown was applied for the 10:00 am – 6:00 pm CST interval on March 12 in Table 5. There are 186 true glitches found in the data, from the 256 triggers PCAT classified. Tables 4 and 5 count only true glitches, not triggers.

Day (2010)	DG	HDG	DG/SS	SS	SN	C (x1)	C (x2)	C (x3)	C (x4)	OG
Feb. 27-28	9	5	2	9	3		1			3
Mar. 11-12	13	3	12	9	7	1				16
Mar. 12-13	4	4	4	11	8					2

Table 4: Breakdown of main glitch classes per 6:00 pm – 2:30 am time interval

Day (2010)	DG	HDG	DG/SS	SS	SN	C (x1)	C (x2)	C (x3)	C (x4)	OG
Mar. 12	10	3	4	12	9	10	5	1	2	4

Table 5: Breakdown of main glitch classes for March 12 10:00 am – 6:00 pm

DISCUSSION

PCAT's calculated efficiency of about 60% indicates that the software may be a useful tool for correctly identifying and classifying glitches. However, more tests may be required on larger collections of data to accurately classify glitches. Clustering the PCAT triggers on a suitable time window would increase the efficiency. The software is most useful where it is complemented with Omega Scans [14].

PCAT will continue to be developed by Dr. Cavaglià, and students and collaborators in the University of Mississippi LIGO group to increase its classifying efficiency. Noise isolation is one of the main drivers of the sensitivity of the LIGO interferometers and the better we can identify these noise events, the more LIGO's astrophysical searches can be improved.

The temporal density of the glitches may help shed light on their origin. Figures 13, 14, and 15 show an even distribution of DGs and HDGs on the nights of February 27-28 and March 11-12 and the afternoon of March 12. There were about half as many DGs and HDGs on the night of March 12-13.

DGs and HDGs were distributed mostly evenly throughout the night of February 27-28, with small concentrations near 9:00 pm and 11:30 pm local time. No DGs or HDGs were found after 1:00 am CST. Several SSs were found between 10:00 and 11:30 pm on the same night, along with a cross doublet and three similar very loud OGs (frequency lines of 50 Hz, 100 Hz, and ~170 Hz). Two of these same glitches were found on the night of March 11-12 (8:40:31 pm and 1:01:53 am CST) and one on the afternoon of March 12 (12:52:30 pm CST).

The night of March 11-12 held the most varied activity among the three nights, with 8 different types of outlier glitches found along with the rest of the glitches. A strong concentration of DGs and DG/SSs were found just after 7:00 pm, 9:30 pm, and 10:00 pm CST. During the first concentration of DGs and DG/SSs, no glitches of another kind were found. However, following this concentration after 7:00 pm CST, 10 outlier glitches of varying nature were found between 7:50 and 9:00 pm CST mixed in with other non-DGs and one DG. Many of these outlier glitches fall into two categories and do not appear at any other time in the data. These glitches often display noisy time series and have irregular shape. The next concentration of DGs after 9:30 pm CST is followed by a spurt of three SSs within 10 minutes of the DGs. The third concentration of DGs between 10:05 pm and 10:25 pm CST is followed by three SNs and two of the same OGs between 10:43 pm and 10:45 pm CST. These two OGs showed frequency lines spanning the spectrogram at ~100 Hz, ~200 Hz, and ~300 Hz.

The night of March 12-13 showed very little activity in the first three hours, with only one SN early and one HDG before 9:00 pm CST. Two concentrations of DGs were found around 9:30 pm CST and just after 1:00 am CST. In this final night, only one type of OG was found and no "cross" glitches were found. The temporal density of the DGs was not constant throughout the three nights but some concentrations emerged between 9:30 and 10:30 pm CST for each night.

The afternoon of March 12 contained the vast majority of the "cross" glitches in varying form and concentration. The density of DGs is similar to the first night of the three-night data run. Between 12:03 and 12:05 pm CST, four "cross" singlets and 3 "cross" doublets were preceded by an SS and followed by an SN. Five of the same OGs

were also found along the time plot with no consistent pattern. Strangely, no glitches of any kind were found between 1:00 and 2:00 pm CST. A massive concentration of "cross" glitches and others were found between 3:00 pm and 5:00 pm, most notably five "cross" singlets, two doublets, one triplet, and two quadruplets. This data was useful in determining if DGs were present during the day as well as during the night, which they were.

While no consistent pattern emerged from plotting the times of the various glitches, it would be interesting to compare the time plot with the interferometer log activity, which records anthropogenic activity, seismic events, and other notable activity in the area of the interferometer.

CONCLUSION

In this project, LIGO's data from the S6 science run were analyzed using Principal Component Analysis for Transients (PCAT) and Omega Scans to provide insight on the nature of some noise transients and test software developed by the University of Mississippi LIGO group. The software was able to identify glitches of different origin in the data. However, analysis of the data found no consistent pattern of glitches. Information of the frequency, amplitude, and duration of the glitches was catalogued to give an encompassing view of data containing "dart" and other glitches in the analyzed period. Our analysis shows that PCAT has an efficiency of 60% or higher in correctly classifying glitches. Thus, PCAT may be a viable tool for detector characterization, though it is most effective when it is complemented by Omega Scans. The work in this thesis represents only an example of the many techniques that are used by LIGO researchers in Detector Characterization. These techniques will continue to improve the sensitivity of interferometers, and further work in the field of detector characterization will be a driving force in increasing the probability of detecting gravitational waves of astrophysical origin.

REFERENCES AND SOURCES

[1]   Aasi, J. *et al.* "Search for gravitational waves from binary black hole inspiral, merger, and ringdown in LIGO-Virgo data from 2009–2010." Phys. Rev. D 87, 022002. 23 January 2013. (and references therein)

[2]   Abadie. J. *et al.* "All-sky search for gravitational-wave bursts in the second joint LIGO-Virgo run." Phys. Rev. D 85, 122007. 20 June 2012. (and references therein)

[3]   Aasi, J. *et al.* "Gravitational Waves from Known Pulsars: Results from the Initial Detector Era." 2014. *Astrophysical Journal. Vol.* 785. 119. (and references therein)

[4]   Abadie, J. *et al.* "Upper limits on a stochastic gravitational-wave background using LIGO and Virgo interferometers at 600–1000 Hz." Phys. Rev. D 85, 122001. 4 June 2012. (and references therein)

[5]   Weisberg, J. M., and J. H. Taylor. "The Relativistic Binary Pulsar B1913+16: Thirty Years of Observations and Analysis." *Binary Radio Pulsars* Ed. F. A. Rasio and I. H. Stairs. *Astronomical Society of the Pacific Conference Series* 328 (2005): 25-31.

[6]   Ade, P. A. R. *et al.* "BICEP2: Detection of B-mode Polarization at Degree Angular Scales." *BICEP2 2014 Results Release*. 18 Mar. 2014.

[7]   Abramovici, A. *et al.* "LIGO: The Laser Interferometer Gravitational-Wave Observatory." *Science* 256.5055 (1992): 325-33.

[8]   Abbott, B. P. *et al.* "LIGO: The Laser Interferometer Gravitational-Wave Observatory." *Reports on Progress in Physics*. Institute of Physics Publishing. 72.076901 2009.

[9]   Buskulic, Damir, and Ilya Mandel. "LIGO and Virgo Gravitational-Wave

Detectors and Their Scientific Reach." Presented at Cracow School for Theoretical

Physics, Zakopane, Poland. 15 Nov. 2013.

[10]   Harry, Gregory M. (for the LIGO Scientific Collaboration) "Advanced LIGO: the

next generation of gravitational wave detectors." 2010. *Class. Quantum Grav.* Vol. 27.

084006.

[11]   Abadie, J. *et al.* "Predictions for the rates of compact binary coalescences

observable by ground-based gravitational-wave detectors." 2010. *Class. Quantum Grav.*

Vol. 27. 173001.

[12]   Official Strain Sensitivities of LIGO Livingston and Hanford Observatories for

Science Run 6 found at http://www.ligo.caltech.edu/~jzweizig/distribution/LSC_Data/

[13]   Cavaglia, Marco, and Trifiro, Daniele. "Characterization of LIGO Noise

Transients with Principal Component Analysis." LIGO Document Control Center (LIGO-

T1300001-v1). 11 Feb. 2013.

[14]   Chatterji, S. K. The search for gravitational-wave bursts in data from the second

LIGO science run. PhD Thesis. MIT Dept. of Physics. 2005. LIGO Document P050033.

[15]   Advanced LIGO Schematic Diagram of PEM Sensors found at

http://pem.ligo.org/

[16]   Christensen, Nelson. "LIGO S6 Detector Characterization Studies." *Classical and

Quantum Gravity.* Institute of Physics Publishing. 21 Sept. 2010.

[17]   Isogai, Tomoki. "Used percentage veto for LIGO and virgo binary inspiral

searches." 2010. *J. Phys.: Conf. Ser.* Vol. 243 012005

[18]   McIver, Jessica. "Data quality studies of enhanced interferometric gravitational wave detectors." 2012. *Class. Quantum Grav.* Vol. 29 124010

[19]   Smith, Joshua R *et al.* "A hierarchical method for vetoing noise transients in gravitational-wave detectors." 2011. *Class. Quantum Grav.* Vol. 28 235005

[20]   Macleod, D. M. *et al.* "Reducing the effect of seismic noise in LIGO searches by targeted veto generation." 2012. *Class. Quantum Grav.* Vol. 29. 055006